Available online at www.sciencedirect.com
SCIENCE DIRECT®
International Journal of Thermal Sciences 43 (2004) 1141–1151
International Journal of Thermal Sciences
www.elsevier.com/locate/ijts

Transition to turbulence: The case of a pipe in radial oscillations

B. Benhamou [a], A. Laneville [b,*], N. Galanis [b]

[a] *LMFE, Department of Physics, Faculty of Science Semlalia, P.O. Box 2390, Marrakech 40001, Morocco*
[b] *Génie Mécanique, Faculté de Génie, Université de Sherbrooke, Sherbrooke, QC, Canada J1K 2R1*

Received 14 August 2003; received in revised form 2 March 2004; accepted 4 March 2004

Available online 28 May 2004

Abstract

This paper deals with an experimental study on flows in a pipe forced to oscillate horizontally about a vertical axis through the center of its inlet section. The study is concerned with the laminar and transition flow regimes and the flow is investigated using streak lines as a visualization technique. According to a similitude analysis, four criteria govern this phenomenon: the flow Reynolds number, the oscillations Reynolds number (or the reduced frequency), the oscillations amplitude and the Euler number. This paper is mainly concerned with the effects of the oscillations and the flow Reynolds numbers. The results show that the pipe oscillations destabilize the laminar flow: the straight streak line observed in the case of a stationary pipe undergoes a bending and then deforms into an *S* shape; the longitudinal location of these flow events correlates with both Reynolds numbers. The pipe oscillations are also observed to induce an earlier transition from the laminar to the turbulent regimes; again, the flow and oscillations Reynolds numbers determine the flow regime present in the oscillating pipe. A chart based on the results of 130 tests is proposed to define the conditions of these regimes.

Introduction

The laminar flow of a fluid within a horizontal pipe subjected to radial oscillations is examined in laboratory tests. The axis of oscillations is vertical, orthogonal to the pipe's axis and located at its inlet. This problem is of interest especially in the case of internal flows in moving systems such as ships. The pipe oscillations induce a transverse motion of the fluid and, as established in similar problems [1], this secondary motion can play an important role in heat or mass transfer devices. It can indeed increase the rate of both transfers by redistributing some of the heat and mass from the pipe wall to its centre. If the flow conditions are such that the maximum axial velocity occurs near the pipe axis, convection of heat and mass is enhanced [2]. A momentum balance on the fluid particles shows that the motion of the pipe generates tangential and Coriolis forces that are functions of the direction of the oscillatory pipe motion and of the position of the fluid particles; more complexity is then expected in the flow field. The flow structure, the resistance to the fluid flow, as well as the transition to turbulence, may consequently be modified. The present experimental study adopts a simple flow visualization technique to investigate the effect of the pipe oscillations. The objective is to answer the questions:

(i) What are the flow modifications in the laminar regime due to the pipe oscillations?
(ii) Is transition promoted by the pipe oscillations?

This work is the experimental companion to previous numerical studies [3–7] on this subject on which little is found in the literature.

1. Description of the phenomenon and first analysis

Although the laminar flow of a fluid in a circular pipe and its transition from the laminar to the turbulent regimes is a well-studied phenomenon, the superposition of radial oscillations to the entire pipe and consequently the imposition of a time-varying boundary condition bring new facets to the picture of the classical case. The criteria of similitude are first determined from a dimensional analysis

* Corresponding author. Fax: (819) 821 7163.
E-mail addresses: bbenhamou@ucam.ac.ma (B. Benhamou), andre.laneville@usherbrooke.ca (A. Laneville).

1290-0729/$ – see front matter
doi:10.1016/j.ijthermalsci.2004.03.006

Nomenclature

D	internal diameter of the test section (3.78 cm)
e	internal surface roughness of the test section (smooth Plexiglas)
Eu	Euler number, $= \frac{\Delta p D^4}{\rho Q^2}$ or $\frac{\Delta p}{\rho \overline{U}^2}$
F_R	reduced frequency, $= \frac{Re_\omega}{Re} = \frac{\omega D}{\overline{U}}$
g	acceleration of gravity
L	length of the test section (4.78 m)
Q	volume flow rate
r, θ, z	cylindrical polar coordinates
t	time
U	flow mean velocity
V_r, V_θ, V_z	local instantaneous velocities in cylindrical polar coordinates
Z_S	longitudinal location of the S shape
Re	flow Reynolds number, $= \frac{\rho D \overline{U}}{\mu}$
Re_ω	oscillations Reynolds number, $= \frac{\rho D^2 \omega}{\mu}$
β, $\beta_{\max}$	instantaneous angular amplitude, its maximum
Δp	static pressure difference between the pipe inlet and outlet
μ, ν	fluid dynamic and kinematic viscosities
ρ	fluid density
ω	oscillations angular frequency

based on the measurable variables and then found to be consistent with the governing equations.

1.1. Dimensional analysis

In the case of laminar and transition flows inside a horizontal pipe which is oscillating in a radial direction, the main variables are

(i) the internal diameter of the pipe, D, its length, L, and roughness height, e,
(ii) the fluid density, ρ, and dynamic viscosity, μ,
(iii) the static pressure difference between the pipe inlet and outlet, Δp, the volume flow rate, Q, the frequency, ω, and angular amplitude, $\beta_{\max}$, of the oscillations, and the acceleration of gravity, g.

Since the energy required maintaining the fluid in motion originates from two sources, a constant head and the time-varying motion of the wall imposed externally, the variables Q and Δp can be expected to be functions of time.

In the particular case of this phenomenon when gravity is neglected, there is only one characteristic mass, but two possible characteristic lengths and three possible characteristic times: $M_C = \rho D^2 L$ or the mass of the fluid contained in the pipe at any instant $L_{C1} = D$ and $L_{C2} = L$

$$T_{C1} = \frac{D^2 L}{Q} \quad \text{or} \quad \frac{L}{\overline{U}}$$

$$T_{C2} = \frac{2\pi}{\omega}, \qquad T_{C3} = \frac{\rho L D}{\mu} \quad \text{or} \quad \frac{\rho D^2}{\mu}$$

T_{C1} corresponds to the convection time of the fluid inside the pipe ($\overline{U}$ is the mean velocity), T_{C2} to the oscillation period of the pipe and T_{C3} to the time of the viscosity diffusion process. The standard convective Reynolds number for an internal flow is obtained by the ratio of T_{C3} and T_{C1} and the oscillations Reynolds number by the ratio of T_{C3} and T_{C2}:

$$Re = \frac{\rho D \overline{U}}{\mu}, \qquad Re_\omega = \frac{\rho D^2 \omega}{\mu}$$

The same results are obtained by the conventional application of the Pi theorem. On the other hand, the reduced frequency can be defined from the ratio of the Reynolds numbers:

$$F_R = \frac{Re_\omega}{Re} = \frac{\omega D}{\overline{U}}$$

The resulting independent non-dimensional variables are then Re, L/D, $\beta_{\max}$, Re_ω (or F_R), e/D while the dependant non-dimensional variable, if the pressure drop is taken into consideration, is the Euler number:

$$Eu = \frac{\Delta p D^4}{\rho Q^2} \quad \text{or} \quad \frac{\Delta p}{\rho \overline{U}^2}$$

1.2. Governing equations

The governing equations were previously established in a numerical study of the problem presented in a companion paper [3]. In order to link the similitude criteria to the different forces present in this phenomenon, these governing equations are briefly analysed.

Consider a developing flow in a horizontal pipe which is initially stationary. At $t = 0$ the pipe starts oscillating around its vertical diameter at the entrance ($z = 0$), with an angular velocity:

$$\Omega = \dot{\beta} = \beta_{\max} \omega \cos(\omega t)$$

For a non-inertial frame of reference moving with the pipe, the governing equations can be written in non-dimensional form [3]:

$$\frac{\partial V_r}{\partial r} + \frac{V_r}{r} + \frac{1}{r}\frac{\partial V_\theta}{\partial \theta} + \frac{\partial V_z}{\partial z} = 0$$

$$\frac{\mathrm{D}V_r}{\mathrm{D}t} - \frac{V_\theta^2}{r} = -\frac{\partial P}{\partial r} + \left(\nabla^2 V_r - \frac{V_r}{r^2} - \frac{2}{r^2}\frac{\partial V_\theta}{\partial \theta}\right) - 2[Re_\omega Re\, \beta_{\max}] V_z \cos\theta \cos(Re_\omega t) + \left[Re_\omega^2 Re\, \beta_{\max}\right] z \cos\theta \sin(Re_\omega t)$$

$$\frac{\mathrm{D}V_\theta}{\mathrm{D}t} + \frac{V_r V_\theta}{r} = -\frac{\partial P}{r\partial\theta} + \left(\nabla^2 V_\theta - \frac{V_\theta}{r^2} + \frac{2}{r^2}\frac{\partial V_r}{\partial\theta}\right) + 2[Re_\omega Re\,\beta_{\max}]V_z \sin\theta\cos(Re_\omega t) - \left[Re_\omega^2 Re\,\beta_{\max}\right] z\sin\theta\sin(Re_\omega t)$$

$$\frac{\mathrm{D}V_z}{\mathrm{D}t} = -\frac{\partial P}{\partial z} + \nabla^2 V_z + \left[2\frac{Re_\omega}{Re}\beta_{\max}\right](V_r\cos\theta - V_\theta\sin\theta)\cos(Re_\omega t) - \left[\frac{Re_\omega^2}{Re}\beta_{\max}\right] r\cos\theta\sin(Re_\omega t)$$

In the momentum equations, the parameters $Re_\omega Re\,\beta_{\max}$ and $Re_\omega^2 Re\,\beta_{\max}$ indicate, respectively, the effect of the Coriolis and tangential forces in the radial and azimuth planes at any given cross-section of the pipe. The ratios $Re_\omega\,\beta_{\max}/Re$ and $Re_\omega^2\,\beta_{\max}/Re$, appearing in the axial momentum equation, are a combination of the reduced frequency and the angular amplitude. These ratios represent, respectively, the effect of the Coriolis and tangential forces in the z-direction.

2. Experimental set-up

2.1. Description

The experimental apparatus consists of a test section, a hydraulic supply system and a scotch yoke mechanism (Fig. 1). The test section is a 4.78 m long Plexiglas pipe with a 3.78 cm internal diameter. The hydraulic supply system consists of a constant head tank and a settling chamber. The fluid flows from the settling chamber to the pipe via a profiled nozzle. The conditions required at the pipe inlet are those set in the numerical simulations: $z = 0$ is a location where the velocity profile is uniform, where the flow is free of turbulence and of any perturbations due to the mean flow, and furthermore, it is the location of a vertical axis of rotation. These conditions cannot be achieved perfectly in the experimental set-up. The addition of a short and high contraction ratio nozzle upstream of the pipe inlet dampens the intensity of the perturbations present in its inlet flow by the square of the contraction ratio (this ratio is 9 in the set up), in addition to producing a uniform velocity profile outside a thin boundary layer. Since the nozzle is attached to the pipe, it oscillates slowly in the settling chamber. For a period of oscillation ($\beta_{\max} =$ 8.4 deg), the displacement at the nozzle inlet wall varies between $-D/4$ and $D/4$ from the stationary position: the intensity of the velocity perturbation (produced at the inlet wall) relative to the mean velocity can be shown to diminish by a factor of 81 (the square of the nozzle contraction ratio) as the flow exits the nozzle and enters the test section. Taking into consideration the length of the nozzle ($1.75\,D$) and the ratio of the flow velocity to the pipe oscillation velocity, the intensity of the perturbations close to the wall at the pipe inlet can be estimated as

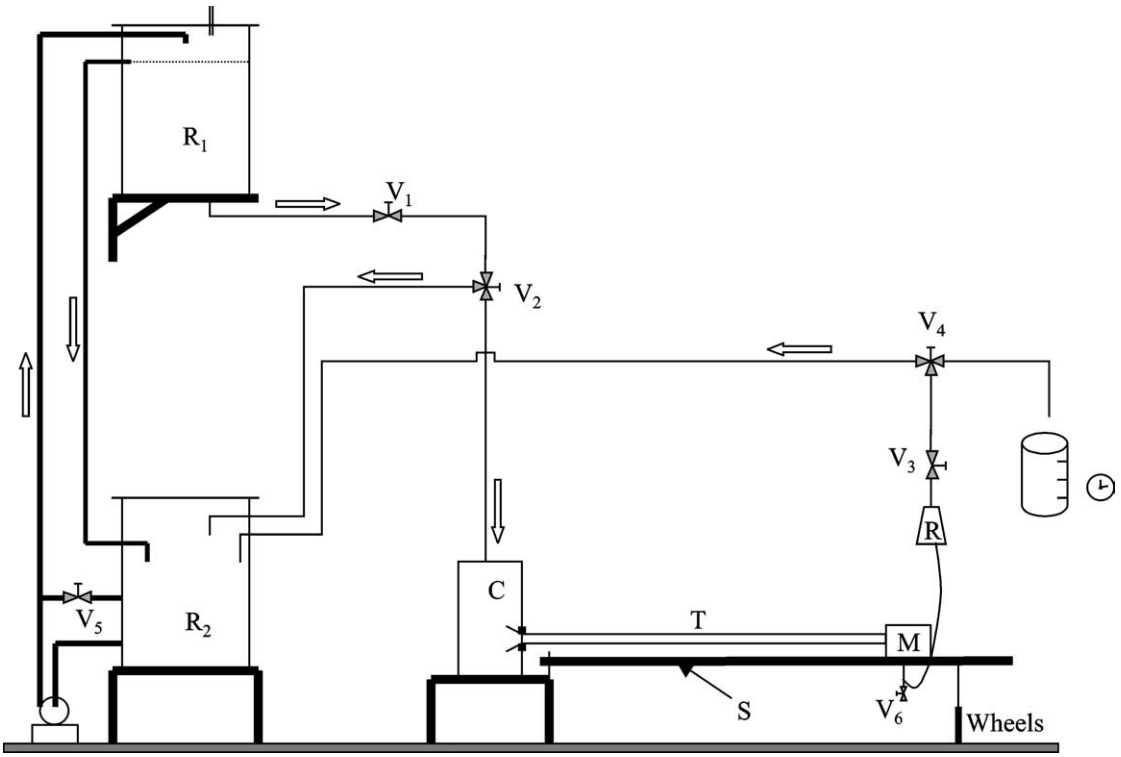

Fig. 1. Experimental set-up. C, M, R, R_1, R_2, S and T are, respectively, the settling chamber, the bulk conditions measurement chamber, the flow meter, the constant head reservoir, the overflow-return reservoir, the test section support and the test section. Valves V_1 to V_6 control the flow, either its rate or its direction. V_4 is used to calibrate the flow meter.

$0.0375\,Fr$. For most of the tests, the value of Fr is less than 1 and the effect of the moving wall at the nozzle inlet is considered to be less important. This was confirmed experimentally: the streak line originating at $z = 0$ showed no local curvature.

A portion of the wall of the stationary settling chamber was replaced by a flexible membrane; this membrane acts as a joint between the stationary chamber's wall and the nozzle and allows for the relative motion of the nozzle-pipe assembly. The pipe is mounted onto a table, the upstream end of which is attached to the stationary settling chamber support by means of two ball bearings. Two low-friction wheels carry the table at the downstream end. The system is supplied with water the flow rate of which is set using a needle valve and a rotameter. The mass flow rate is determined by weight. Uncertainty in the case of the value of the measured Re is always less than 3%.

The sinusoidal oscillations of the pipe around its vertical axis at the entrance are obtained using a scotch yoke mechanism driven by a variable speed motor. The resulting uncertainty in the case of the measured Re_ω is less than 3%.

Fig. 2 shows a sketch of the visualization set-up. The flow is visualized by injecting a fluorescent dye and illuminating the pipe with a 600 W halogen light. The dye injection set-up consists of a reservoir that delivers the dye (solution of 2 g of fluorescein sodium salt in 1 L of water [8]) to the injection tube, a 1.8 mm external diameter brass capillary tube mounted on the nozzle and extending to the test section inlet. A flexible piece of tubing links the reservoir to the injection tube. To insure that the pressure at the injection point does not differ from that of the pipe flow, the dye reservoir is connected to the water supply immediately upstream of the settling chamber. The injection tube is inserted at the geometric center of the pipe through the settling chamber and the dye is released at 7.4 cm downstream of the pipe inlet. A valve located at the outlet of the dye reservoir allows for the regulation of the dye flow rate. The images of the streak lines produced by the tracer

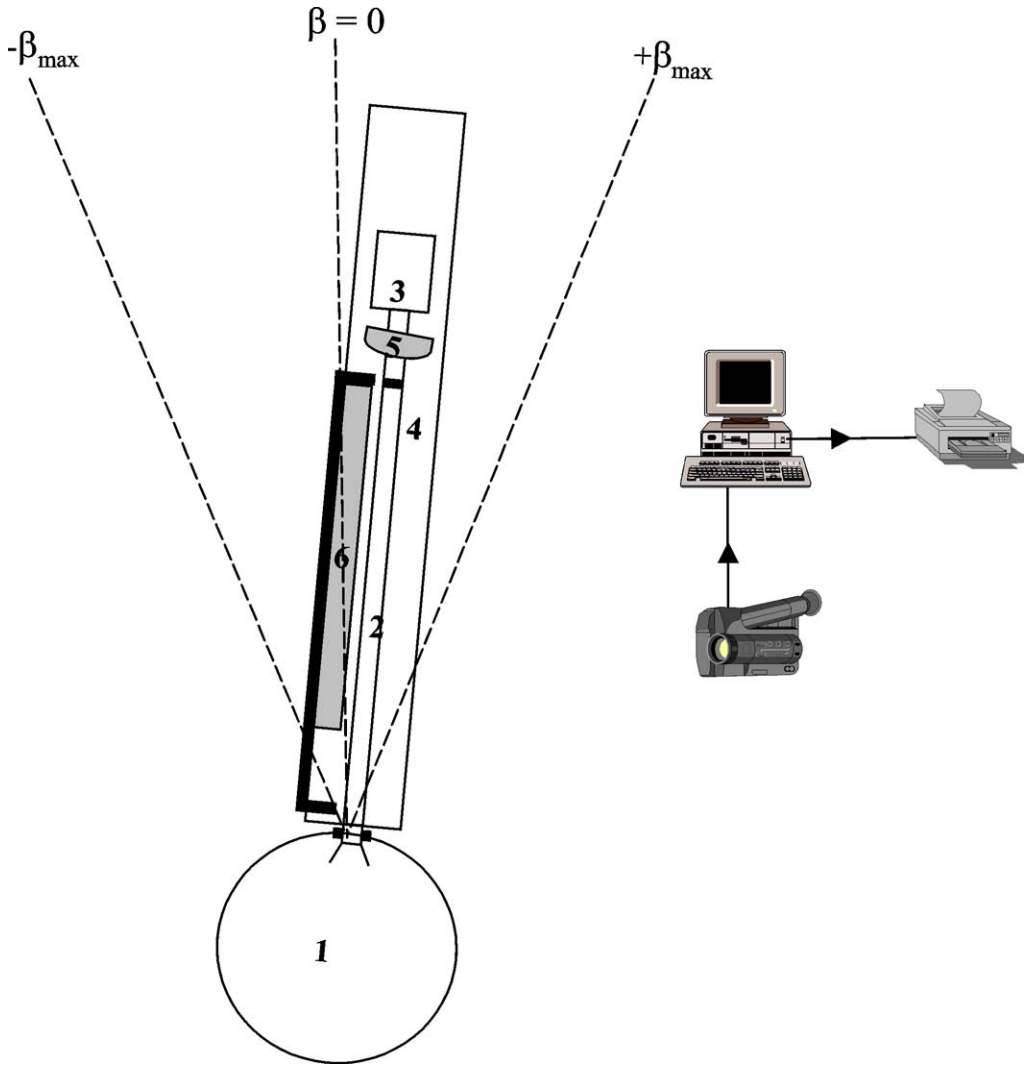

Fig. 2. Visualization set-up. The identification of the different components is: **1** the settling chamber, **2** the test section, **3** the bulk conditions measurement chamber, **4** the test section support, **5** the halogen light source and **6** top view mirror. The line $\beta = 0$ corresponds to the reference axis.

are captured using a video camera mounted 2.5 m from the test section. The flow is visualized over a length of 138 cm (approximately 36 pipe diameters).

2.2. Test conditions

In the case of the tests with the pipe in forced oscillation, the flow Reynolds number Re was varied from 210 to 2313 and the oscillation Reynolds number Re_ω , from 242 to 2788. The angular amplitude of the pipe oscillations was set at $\beta_{\max} = 8.4°$, a value imposed by space limitations in the laboratory.

The objective of this paper is to show the effects of pipe oscillations on the laminar flow and its transition to turbulence. An overall description of the visualization is given for some combinations of the two Reynolds numbers and an analysis of the details of the flow follows.

3. Results

3.1. Stationary pipe

In the case of the stationary pipe, a streak line of tracer, as it will be illustrated later in Fig. 4(a), displays a low frequency wave in the range $2313 \leqslant Re \leqslant 2498$. The frequency of this wave increases with Re but no turbulent mixing is detected. Significant but intermittent mixing of the flow begins for $Re = 2602$ and, steady mixing occurs for $Re = 3852$.

3.2. Forced oscillations

Two values of Re (1388 and 2313) were selected to illustrate the effects of the pipe oscillation (or Re_ω) on the flow. As a corollary, the effect of the volumetric flow rate (or Re) on the flow regime is examined for two values of Re_ω (1013 and 2788). Comments on the corresponding results follow.

3.2.1. The effect of Re_ω in the case of $Re = 1388$

When the pipe is stationary, as expected the visualized streak line remains on the pipe axis and the flow is laminar (Fig. 3(a)). In Figs. 3(b)–(f) the pipe oscillates with different frequencies. These pictures correspond to the pipe position $\beta = +8.4°$.

In the case of an oscillation frequency such as $Re_\omega = 411$, the visualization video shows that the streak line resulting from the injected dye has a helicoidal form and its time evolution appears to be periodic. The axis of this helicoidal form is located on the pipe axis. The helicoidal shape of this streak line is due to the secondary flow induced by the pipe oscillations [3,6,7]. The flow remains laminar (Fig. 3(b)).

For $Re_\omega = 641$, the shape of the streak line is no longer helicoidal over the entire length of the pipe, especially near the pipe exit. Indeed, the trace adopts an S shape that can be clearly seen on Fig. 3(c). This aspect of the phenomenon will be considered in more detail later. Even in the presence of the S shape, the streak line is well defined and does not exhibit any turbulent mixing: the flow is considered to remain laminar.

For a pipe oscillation frequency such that $Re_\omega = 1365$ (Fig. 3(d)), the time evolution of the streak line is not periodic over the entire length of the pipe: the S shape is formed further upstream and dispersion of the trace follows and finally occupies the whole cross section of the pipe at about $z/D = 23$. Near the pipe exit (about $z/D \geqslant 36$), the flow structure evolves intermittently between a well-ordered and disordered structure. In the case of the ordered structure, the dye filament slips along the pipe length despite the fact that it is dispersed: the flow evolves between laminar and turbulent structures, so it is in transition to turbulence.

For pipe oscillation frequencies in the range $641 < Re_\omega \leqslant 2788$, the flow patterns resemble that of $Re_\omega = 641$, but the disordered structure occurs more frequently and at axial positions closer to the pipe entrance as Re_ω is increased (Figs. 3(d)–(f)).

3.2.2. The effect of Re_ω in the case of $Re = 2313$

In the case of a stationary pipe (Fig. 4(a)) the visualized streak line is well defined but slightly unstable. This corresponds to the upper limit of laminar flow. In Figs. 4(b)–(f) the pipe oscillates with different frequencies. Again these pictures correspond to the pipe position $\beta = +8.4°$.

For $Re_\omega = 242$, the flow patterns are similar to those observed in the case of $Re_\omega = 641$ and $Re = 1388$ (Figs. 3(c) and 4(b)). The flow is laminar.

For $Re_\omega = 411$, the visualized streak line continues to be well defined near the pipe entrance. However, near the pipe exit, it evolves intermittently between well-ordered and disordered structures (Fig. 4(c)) as in the case of $Re_\omega = 1365$ and $Re = 1388$ (Fig. 3(d)). The latter structure results from the presence of turbulent vortices. This flow pattern is a characteristic of transition to turbulence [9].

As Re_ω is increased further (Fig. 4(d)), the disordered structure is more present during an oscillation cycle and occupies a longer section of the pipe. The flow continues its transition.

For $Re_\omega = 1013$, the turbulent structures cease to be intermittent. Due to turbulence the dye thread diffuses into the stream and the fluid becomes uniformly colored near the pipe exit (Fig. 4(e)). The turbulent region tends to stretch along the whole length of the pipe as Re_ω is increased. Indeed, the flow becomes fully turbulent along the pipe length for $Re_\omega = 2788$ (Fig. 4(f)).

3.2.3. The effect of Re in the case of $Re_\omega = 1013$

Fig. 5 shows the effect of the flow Reynolds number on the flow patterns at a fixed pipe oscillation frequency ($Re_\omega = 1013$). For $Re = 922$, the visualization results show a helicoidal streak line near the pipe entrance. However, far from the pipe entrance, this streak line adopts an S shape

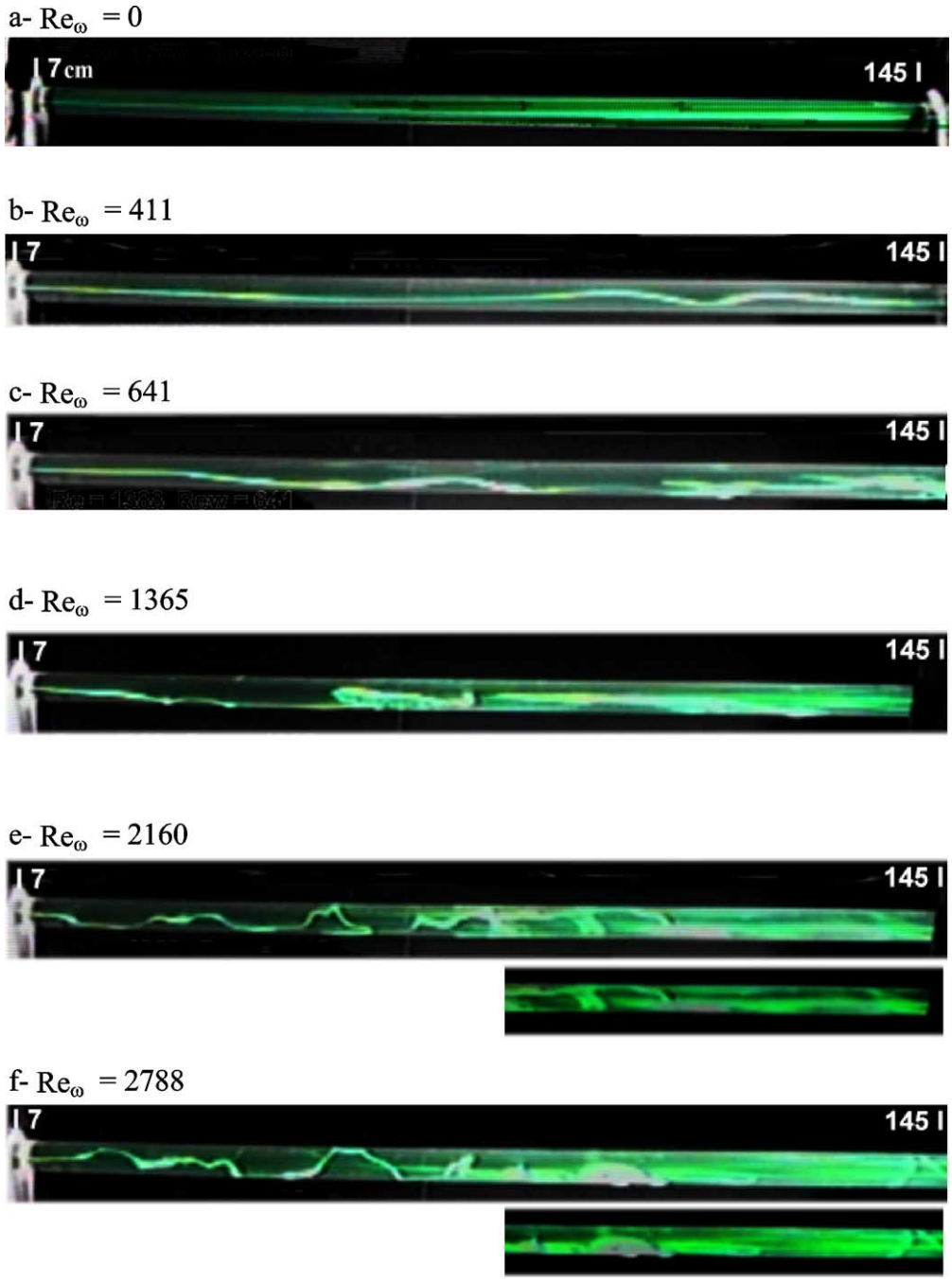

Fig. 3. Flow patterns for $Re = 1388$ and $\beta = 8.4°$.

and, further downstream, is dispersed by friction along the pipe wall (Fig. 5(a)). Despite these events, the dye filament does not present any mixing and the flow is considered to remain laminar as in Figs. 3(c) and 4(b). In contrast, in the case of $Re = 1846$ the streak line presents some turbulent vortices. The zoom of Fig. 5(b) clearly shows these vortices. However, they are not present during the whole oscillation cycle. It is then a case of flow in transition to turbulence such as in Figs. 3(d)–(f) and 4(c)–(d). In the case of $Re = 2313$ (Fig. 5(c)), turbulent vortices are present during the entire oscillation cycle. These vortices induce a large mixing of the flow that becomes uniformly colored downstream as illustrated on the zoom picture of Fig. 5(c). This flow is then turbulent like the cases in Figs. 4(e)–(f).

3.2.4. The effect of Re in the case of $Re_\omega = 2788$

Fig. 6 shows flow patterns for $Re_\omega = 2788$ that resemble those observed in the case of $Re_\omega = 1013$ at the corresponding Re. However the flow structure at $Re_\omega = 2788$ is more destabilized than the one at $Re_\omega = 1013$ as can clearly be seen by comparing Figs. 5(a) and 6(a), (b), 5(b) and 6(c), 5(c) and 6(d). The visualization results show that the flow

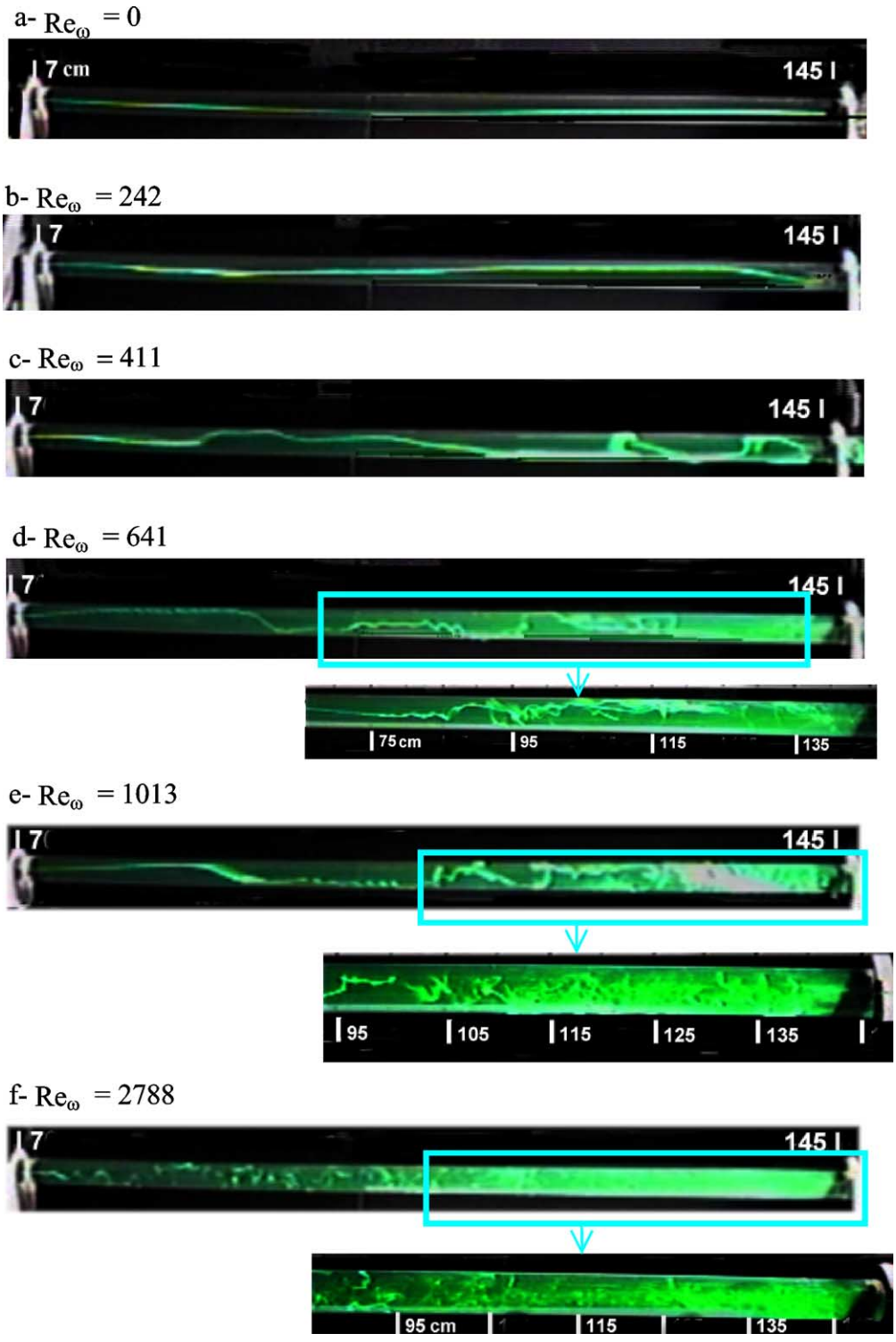

Fig. 4. Flow patterns for $Re = 2313$ and $\beta = 8.4°$.

at $Re = 922$ and 1142 is laminar but includes some S shape that destroys the helicoidal form of the visualized streak line. Then, for $Re = 1846$, the flow is in transition with intermittent turbulent vortices and finally, for $Re = 2313$, the turbulent vortices are present permanently.

3.2.5. Four types of flows

An analysis based on the comments of the previous section and on additional visualization videos, permits us to define four main types of flow for the considered tube length ($L/D = 126.4$):

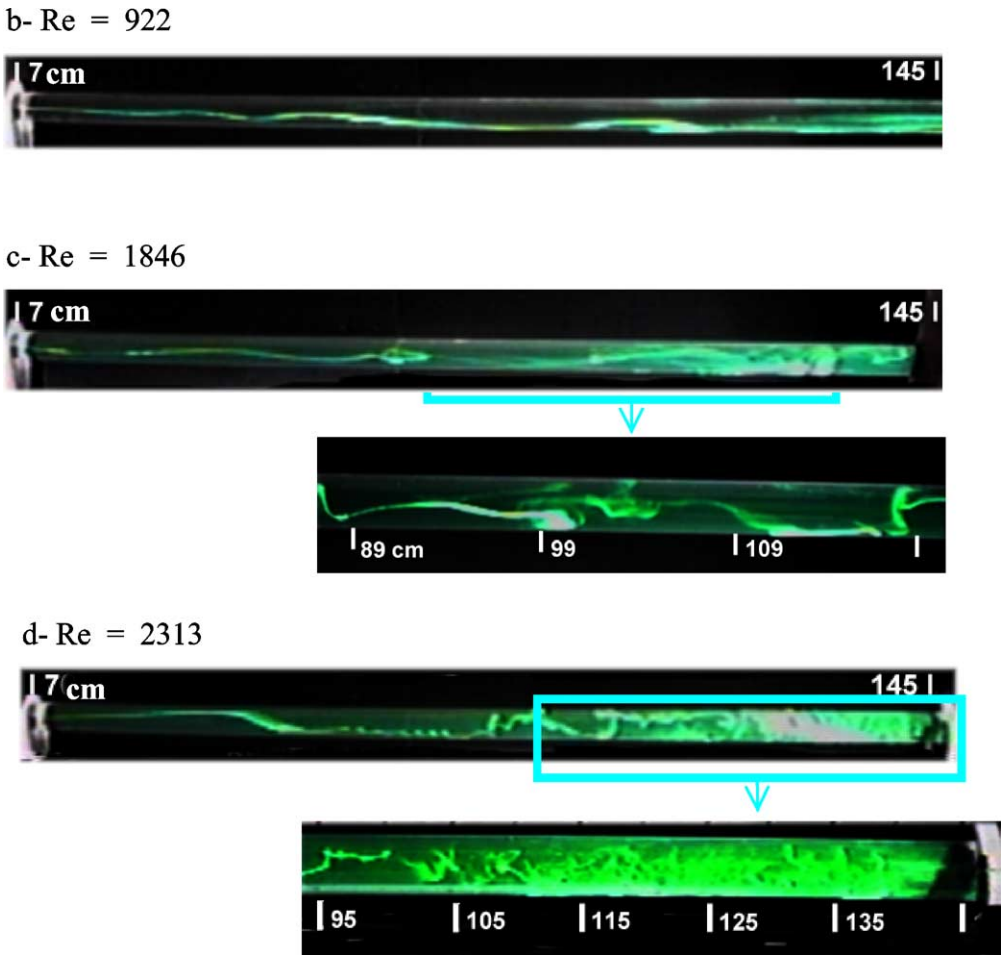

Fig. 5. Flow patterns for $Re_\omega = 1013$ and $\beta = 8.4°$.

Type I: This type is characterized by a streak line that develops periodically as the fluid flows downstream. The geometry of this streak line is helicoidal and the overall flow remains laminar. This type of flow is shown in Fig. 3(b).

Type II: In this flow type, the streak line ceases to have a periodic evolution, especially near the pipe exit. This streak line includes an *S* shape within the length of the pipe. This *S* shape will be discussed later. Even if this shape is present in the streak line, the flow does not exhibit turbulent mixing and is considered to remain laminar. This type of flow is illustrated in Figs. 3(c), 5(b), 6(a) and 6(b).

Type III: The streak line in this case evolves chaotically. As it approaches the pipe exit the tracer becomes blurred. The overall flow in this region is intermittent, changing from organized (laminar) to disorganized patterns. In the case of disorganized conditions, large structures are present and transverse mixing of the flow produces a uniform color of the fluid. This type of flow is defined as one of transition and is shown in Figs. 3(d)–(f), 4(c)–(d), 5(c) and 6(c).

Type IV: As opposed to type III, this flow is characterized by permanent turbulent structures, and transverse mixing makes the fluid uniformly colored. This type of flow is considered to be turbulent. Figs. 4(e)–(f), 5(d) and 6(d) illustrate type IV flow. Transverse mixing induced by the pipe oscillations is also clear on Fig. 7.

Visualization results show that flows of type III are not laminar and those of type IV are turbulent. This clearly establishes that pipe oscillations induce an earlier transition to turbulence than in the stationary case. This earlier transition is due to the Coriolis force. Indeed, this force induces a transversal flow that causes a strong momentum transfer in a pipe cross-section [3–7]. This transfer extracts energy from the main axial flow and then destabilizes the flow. Schlichting [9] reports some theoretical studies on the stability of laminar flows which assess that the existence of an inflexion point in the axial velocity profile is a sufficient and necessary condition to destabilize the flow. In the case of a laminar flow in an oscillating pipe, numerical simulations [5–7] have established that an axial flow reversal can occur. This flow reversal introduces an inflexion point in the V_z pro-

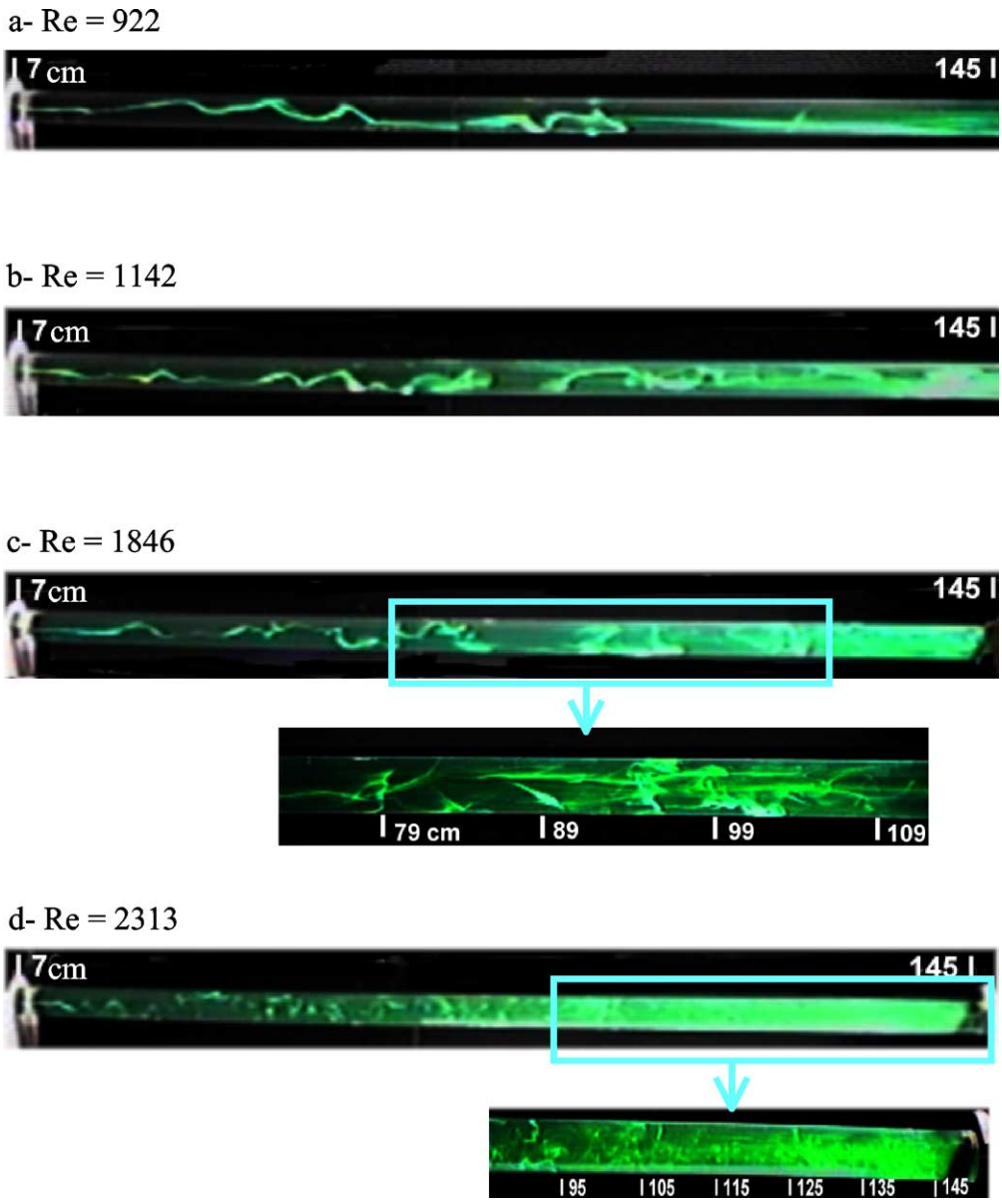

Fig. 6. Flow patterns for $Re_\omega = 2788$ and $\beta = 8.4°$.

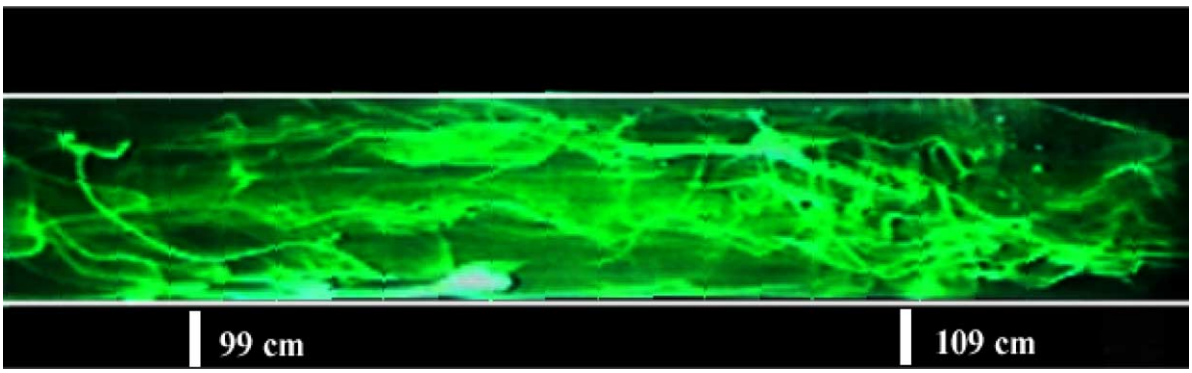

Fig. 7. Turbulence induced by pipe oscillations. $Re = 2070$, $Re_\omega = 2160$ and $\beta = 8.4°$.

file and destabilizes the flow. On the other hand, the early transitions depicted here have been observed in other problems such as Taylor–Couette flow [10,11], oscillating flow in a pipe [12], mixed convection [8] and radial rotation [13]. In the last-mentioned problem, Cheng and Wang [13] have conducted airflow visualization in a radial rotating tube and shown that the Coriolis force can have a destabilizing effect and induce an earlier transition at low flow Reynolds number ($Re = 500$).

3.2.6. Transition chart

To obtain a flow chart indicating the limits of each type of flow in terms of the two Reynolds numbers, many combinations of Re and Re_ω were considered. The result of these visualizations is reported in Fig. 8. This chart shows that pipe

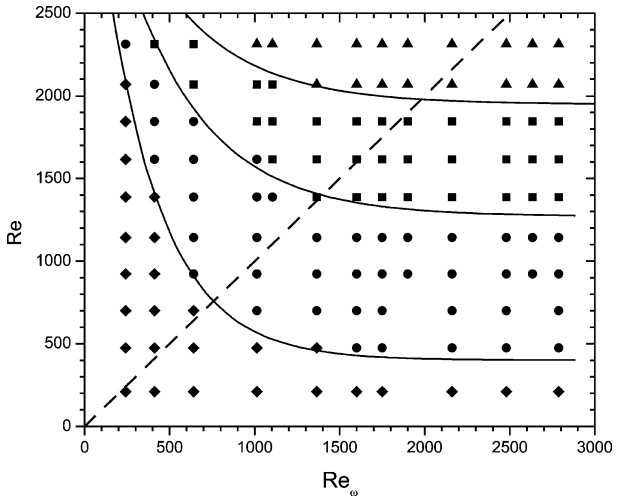

Fig. 8. Chart of transition to turbulence for $\beta = 8.4°$ and $L/D = 126.4$. The dash and solid lines correspond, respectively, to the reduced frequency $F_R = 1$ and boundaries between the different flow types. The symbols indicate the flow types (◆ type I; ● type II; ■ type III; ▲ type IV).

oscillations destabilize the laminar flow, cause many modifications on it and can also induce an earlier transition to turbulence. Indeed, the value of Re for which the flow ceases to be laminar is lower than in the case of a stationary pipe. This critical value of Re decreases as Re_ω is increased. In Fig. 8 the straight line corresponds to the case $F_R = 1$; this line ($Re = Re_\omega$ or $D\omega = U$) intersects the boundary curve between type I and type II at its point of maximum curvature. The onset of the S shape distortion is then particularly influenced by Re_ω if $F_R \geqslant 1$. This effect of Re_ω in the cases of $F_R \geqslant 1$ can be extended to the four types of flow.

3.2.7. Two features of the flow: slope change in the helicoidal line and the S shape

For the cases of low and constant Re, a streak line originating from the pipe inlet center slowly departs from a straight line on the pipe axis into a helicoidal line towards the pipe wall. This helicoidal line can be clearly observed for $Re = 1388$, $Re_\omega = 411$ and 641 (Fig. 3). The first change in the slope of this line from a positive to a negative value occurs, respectively, for $z/D = 26$ ($Re = 1388$, $Re_\omega = 411$) and 19 ($Re = 1388$, $Re_\omega = 641$). This event occurs, but not as clearly, for $z/D = 9$ in the case of $Re_\omega = 1365$. The development of this helicoidal line appears to scale with $Re_\omega z/D$ since the same local event occurs for $Re_\omega z/D = 11\,500$ within 6%.

Further downstream, the helicoidal line forms an S shape, one portion of the fluid at a given z/D moving with a slower axial velocity than the other portion. An enlarged view of the S shape is shown in Fig. 9. This shape has been obtained in additional tests performed to understand the mechanism of generation of the S shape distortion: the dye was injected by means of a capillary tube located at the horizontal plane passing through the pipe axis near the wall. To achieve a front view of the resulting streak line, the video camera was mounted at 1 m from the test section (see Fig. 2). For a top view, a mirror was placed behind the test section at a height of 3 cm from the pipe with a 30° angle relative to a

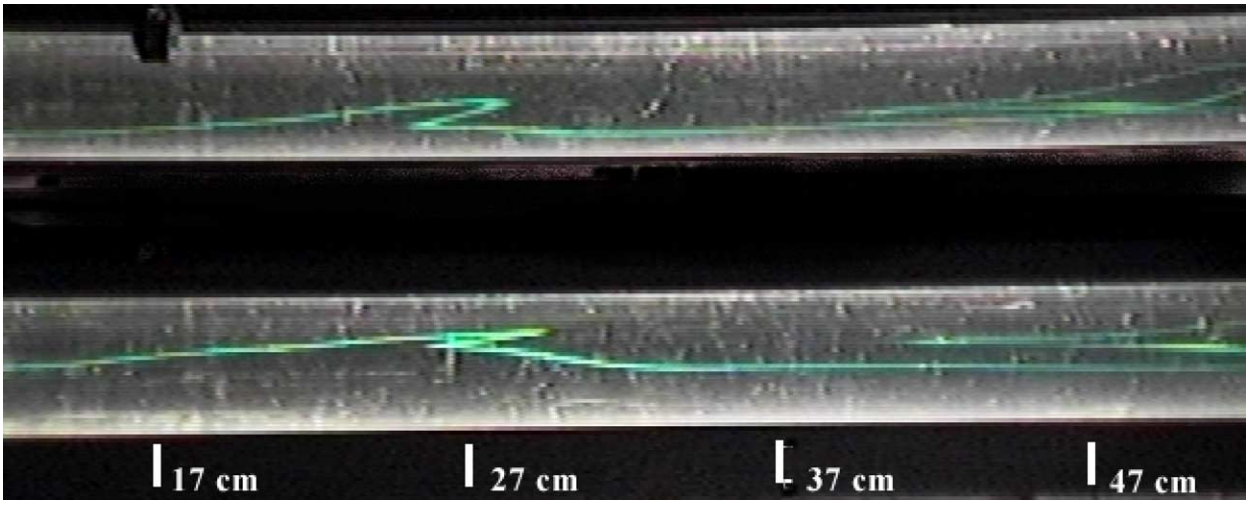

Fig. 9. Top and front views of the S shape distortion. $Re = 1000$, $Re_\omega = 1104$ and $\beta = 8.4°$.

Table 1
Axial location of the S shape distortion

Re_ω	Re	$Re_\omega z_S/D$
641	1388	17563
1365	1388	19383
2160	1388	18511
411	2313	11685
1013	922	24582
1013	1846	16500

vertical plane. Several visualizations were performed and the case of $Re = 1000$, $Re_\omega = 1104$ and $A = 8.4°$ was selected in Fig. 9. The upper picture is the top view. The pipe has left its central position $\beta = 0$ and is moving towards its extreme position $\beta = -8.4°$. The dye injection tube is at the leading edge. The transversal component of the Coriolis force, directed towards the trailing edge [3], pushes the fluid to this side of the pipe. Fluid particles marked by the dye are then pushed towards the pipe center where the axial velocity is important. These particles are accelerated and reach those injected previously.

The occurrence of this distortion of the streak line into an S shape seems to concur again with $Re_\omega z/D$, the most upstream part of the S being located at $Re_\omega z/D = 18\,500$ within 4% (for cases c and d of Fig. 3, $z/D = 27$ and 14). As Re_ω is increased, the different events are forced to occur at an earlier location upstream and over a shorter distance. The distortion into an S shape, for example, according to the rule of $Re_\omega z/D = 18\,500$, should appear at the location $z/D = 8.57$ and 6.64 for $Re_\omega = 2160$ and 2788, respectively. In the figure, the S shape is not recognizable but larger amounts of the tracing fluid can be identified at these two locations.

For the two previous common features, the flow is laminar. For identification purposes, the portion of the flow with a straight and helicoidal line is defined as type I while the portion containing its distortion into an S shape is type II (see Section 4.1). For a given value of Re, the appropriate similitude criterion for local events in these portions of the flow is $\omega z D/\nu$, a Reynolds number based on the local wall velocity. If Z_S is defined as the axial location where the S shape distortion takes place, the data obtained from the visualization are tabulated in Table 1. These data would fit the following empirical relation:

$$Re_\omega \frac{Z_S}{D} = 32\,810 - 9.31Re$$

Downstream of the S shape, the streak line tends to be chaotic and diffuses significantly. The structure of the flow evolves intermittently from organized laminar to disorganized.

4. Conclusion

An experimental visualization has been conducted to examine the developing flow in a pipe forced to oscillate in a horizontal plane. This paper deals mainly with the effect of pipe oscillations on transition to turbulence.

The visualization results show that pipe oscillations induce a secondary transversal flow as indicated by the helicoidal form of the streak lines. At relatively high oscillation frequencies, the intensity of this transversal flow increases and may destabilize the flow structure. Indeed, large mixing is induced in the flow and leads to the development of turbulent vortices even when the flow Reynolds number is lower than its critical transition value for a stationary pipe ($Re < 2000$). This earlier transition to turbulence, attributed to the Coriolis force, occurs at lower values of Re as the oscillation Reynolds number, Re_ω, increases. The flow structure can become fully turbulent if Re_ω is further increased. A chart indicating the limits of the transition and full turbulent flow structures has been established.

Acknowledgements

The authors wish to thank the Natural Sciences and Engineering Research Council of Canada for its financial support.

References

[1] S. Fann, W.-J. Yang, Hydrodynamically and thermally developing laminar flow through rotating channels having isothermal walls, Numer. Heat Transfer Part A 22 (1992) 257–288.
[2] J. Berman, L.F. Mockros, Flow in a rotating non-aligned straight tube, J. Fluid Mech. 144 (1984) 297–310.
[3] B. Benhamou, N. Galanis, A. Laneville, Transient effects of orthogonal pipe oscillations on laminar developing incompressible flow, Internat. J. Numer. Methods Fluids 34 (7) (2000) 561–584.
[4] B. Benhamou, N. Galanis, A. Laneville, Laminar flow in a tube subject to sinusoidal oscillations, in: ECCOMAS '98, Athens, Greece, September 7–11, vol. 1, Wiley, New York, 1998, pp. 1302–1305.
[5] B. Benhamou, N. Galanis, A. Laneville, Numerical study of laminar incompressible flow in an oscillating tube, in: CSME Forum '98, Toronto, Canada, May 19–22, vol. 1, 1998, pp. 169–174.
[6] B. Benhamou, Écoulement dans un tube en oscillations radiales sinusoidales : Étude numérique et visualisation expérimentale, Thèse Ph.D., Université de Sherbrooke, Canada, Juillet 1999.
[7] B. Benhamou, N. Galanis, A. Laneville, Periodic characteristics of laminar developing flow through a tube subject to radial oscillations, Trans. CSME 26 (2) (2002) 219–239.
[8] M.A. Bernier, B.R. Baliga, Visualization of upward mixed-convection flows in vertical pipes using a thin semitransparent gold-film heater and dye injection, Internat. J. Heat Fluid Flow 13 (1992) 241–249.
[9] H. Schlichting, Boundary Layer Theory, McGraw-Hill, New York, 1979.
[10] F. Marques, J.M. Lopez, Taylor–Couette flow with axial oscillations of the inner cylinder: Floquet analysis of the basic flow, J. Fluid Mech. 348 (1997) 153–175.
[11] K.J. Maloy, W. Goldburg, Measurements on transition to turbulence in a Taylor–Couette cell with oscillatory inner cylinder, Phys. Fluids A 5 (1993) 1438–1442.
[12] R. Akhavan, R.D. Kamm, A.H. Shapiro, An investigation of transition to turbulence in bounded oscillatory Stokes flows, J. Fluid Mech. 225 (1991) 395–422.
[13] K.C. Cheng, L. Wang, Transition to turbulence and relaminarization phenomena in rotating radial straight pipes, in: Visualization of Heat Transfer Processes, Atlanta, 29th Nat. Heat Transfer Conf., in: HTD, vol. 252, ASME, 1993, pp. 55–63.